Efficient Wideband Electromagnetic Scattering Computation for Frequency Dependent Lossy Dielectrics Using WCAWE

Patrick Bradley, *Member, IEEE*, Conor Brennan, *Member, IEEE*, and Marissa Condon

***Abstract*—This paper presents a model order reduction algorithm for the volume electric field integral equation (EFIE) formulation, that achieves fast and accurate frequency sweep calculations of electromagnetic wave scattering. An inhomogeneous, two-dimensional, lossy dielectric object whose material is characterized by a complex permittivity which varies with frequency is considered. The variation in the dielectric properties of the ceramic $Ba_xLa_4Ti_{2+x}O_{12+3x}$ in the <1 GHz frequency range is investigated for various values of x in a frequency sweep analysis. We apply the well-conditioned asymptotic waveform evaluation (WCAWE) method to circumvent the computational complexity associated with the numerical solution of such formulations. A multipoint automatic WCAWE method is also demonstrated which can produce an accurate solution over a much broader bandwidth. Several numerical examples are given on order to illustrate the accuracy and robustness of the proposed methods.**

***Index Terms*—Frequency-dependent lossy dielectric, frequency sweep, inhomogeneous, model order reduction, volume electric field integral equation (EFIE), well-conditioned asymptotic waveform evaluation.**

I. Introduction

THE volume electric field integral equation, in conjunction with the method of moments (MoM), is a popular frequency domain technique for analysis of electromagnetic scattering from bodies both of arbitrary shape and inhomogeneity [1]. Many problems, such as the evaluation of the radar cross section (RCS), require the determination of the system response at multiple frequencies. For such analysis, the equivalent current density needs to be calculated at many frequencies. This can be very time consuming when using traditional frequency-domain numerical methods, based on the solution of a dense matrix equation at each frequency [2], [3].

To alleviate this computational burden, several approaches have been proposed [2], [4], [5]. Many of these focus on using a rational function to approximate the solution vector and its derivatives at a central frequency and subsequently exploiting this information to reconstruct the solution within the frequency band of interest. This is possible because coefficients of the system matrix equation, describing the system behavior, are known functions of frequency. The low order of the approximate system matrix permits its inverse to be computed with negligible computational effort. Hence, once the reduced-order system has been constructed, the frequency sweep response can be evaluated at an almost arbitrary number of frequency samples, resulting in a significant reduction in computational cost. Padé via asymptotic waveform evaluation (AWE) [2], [3], [6], passive reduced-order interconnect macro modeling algorithm (PRIMA) and other model-order reduction techniques such as Padé via Lanczos (PVL) [4] have been used for the efficient solution of a wide variety of linear problems. Extending PVL and PRIMA to handle systems with frequency dependence, can prove prohibitive for large-scale computations. Explicit moment-matching such as the Padé via AWE are known to exhibit certain numerical stability problems and are inherently ill-conditioned, inevitably leading to stagnation in the moment-matching process [2], [3], [6], [7]. In this paper, an efficient and numerically stable projection-based algorithm for model order reduction, called the well-conditioned asymptotic evaluation (WCAWE) and originally proposed by [5], is applied to the volume EFIE formulation. This algorithm produces a well-conditioned and high-order approximation from a single expansion point with a significantly wider bandwidth than that obtained from a Padé via AWE and its variants.

Dielectric ceramics are used extensively in microwave devices such as resonators and antennas. These materials are required to have high dielectric constants (ϵ') and low tangent losses $(\tan\delta)$ in order to satisfy the demands of high electrical loads [8], [9]. Due to the precise nature of these devices, it is essential that the frequency dependent fluctuation of the dielectric properties is accounted for in a frequency sweep analysis. Recently, several new microwave dielectric ceramics, with excellent dielectric properties, were reported in [9] and will be used as the basis for this study. The contribution of this variation in the dielectric properties of the ceramic $Ba_xLa_4Ti_{2+x}O_{12+3x}$, in the <1 GHz frequency range, will be investigated for various compositions of the four components [9] (between $x = 0.0$ and 0.2).

Frequency-dependent dielectric variations occur in all materials and typically consist of a decrease in the real and imaginary part of the permittivity as the frequency increases. As discussed in [10], [11] there are several frequency regimes in which the dielectric permittivity is changing. This is due to the fact, that at frequencies up to 1 GHz, the molecules of a material can no longer rotate fast enough to remain in phase with the applied

Manuscript received April 09, 2008; revised October 14, 2008. First published July 28, 2009; current version published October 07, 2009.

The authors are with the RF Modelling and Simulation Group, Research Institute for Networks and Communications Engineering (RINCE), School of Electronic Engineering, Dublin City University, Dublin, Ireland (e-mail: bradleyp@eeng.dcu.ie).

Digital Object Identifier 10.1109/TAP.2009.2028591

field [10], [11]. Consequently, the contribution of the molecular polarization to the net polarization declines, causing a decrease in the dielectric permittivity as the applied field frequency increases.

Over the past decade, much research has been carried out on the electromagnetic characterization of materials over different frequency ranges [12]–[14]. Work in [8], [9], [12]–[14] has tabulated the electromagnetic properties of various materials. In particular the complex dielectric constant and their variation against frequency were noted from empirical measurements.

To the knowledge of the authors, no research to date has examined the wave scattering from a lossy dielectric object with frequency dependent complex permittivity, using the volume EFIE formulations with a model order reduction (MOR) procedure. In particular, the importance of the effect of the frequency dependence of these dielectric properties on the accuracy of a frequency sweep analysis has not been previously researched using MOR.

This paper is organized as follows. In Section II, the volume integral equation formulation is discussed. In Section III, the Asymptotic Waveform Evaluation method is reviewed. Section IV discusses how the frequency dependence of the dielectric properties is accounted for in a frequency sweep analysis. The well-conditioned asymptotic waveform evaluation technique is introduced in Section V, while implementation issues associated with the WCAWE algorithm are analyzed in Section V.A. Numerical results are presented in Section VI. Some concluding remarks and observations are offered in Section VII.

II. Volume Electric Field Integral Equation Formulation

The volume electric field integral equation (VEFIE) formulation is commonly applied to the problem of wave scattering from inhomogeneous objects. The work presented in this paper examines a 2-D TM^z configuration, where scattering structures and fields are assumed invariant in the z-direction. The scattering body is characterized by its permittivity $\epsilon(\mathbf{r})$, conductivity $\sigma(\mathbf{r})$ and we assume constant permeability $\mu(r) = \mu_0$. A time dependence of $\exp(\jmath\omega t)$ is assumed and suppressed in what follows. The object is illuminated by a plane wave and the equivalent polarization currents $J_z(\mathbf{r}) = \jmath\omega(\epsilon_c - \epsilon_0)E_z$ can be expressed in terms of the following electric field integral equation [1]

$$E_z^{\text{inc}}(\mathbf{r}) = \frac{J_z}{\jmath\omega(\epsilon_c - \epsilon_0)} + \jmath\omega\mu_0 \int_v J_z(\mathbf{r}')\frac{1}{4\jmath}H_0^{(2)}(k_b|\mathbf{r} - \mathbf{r}'|)dv' \tag{1}$$

where k_b the background wave number and $H_0^{(2)}$ is the zero-order Hankel function of the second kind. The complex permittivity is given by [15], [16]

$$\epsilon_c(\omega) = \epsilon' - \jmath\frac{\sigma}{2\pi f} = \epsilon' - \jmath\epsilon'' \tag{2}$$

while the real permittivity is given by $\epsilon' = \epsilon_r\epsilon_o$, with ϵ_r being the relative permittivity constant. The imaginary part of the complex permittivity, ϵ'', represents all the dielectric loss of the medium. A measure of the power loss in the medium is given by the ratio [15], [16]

$$\tan\delta_c = \frac{\epsilon''}{\epsilon'} \cong \frac{\sigma}{2\pi f\epsilon'} \tag{3}$$

where δ_c is the loss angle. Both the real and imaginary parts are functions of frequency and are in fact related to each other by the Kramers–Kronig relation [17]

$$\epsilon'(\omega) = \frac{1}{\pi}\mathcal{P}\int_{-\infty}^{\infty}\frac{\epsilon''(\omega_1)}{\omega_1 - \omega}d\omega_1 \tag{4}$$

$$\epsilon''(\omega) = -\frac{1}{\pi}\mathcal{P}\int_{-\infty}^{\infty}\frac{\epsilon'(\omega_1)}{\omega_1 - \omega}d\omega_1 \tag{5}$$

where $\mathcal{P}$ means that the Cauchy principal value of the integral is used. The dependence of the real and imaginary parts of ϵ on frequency is clearly evident in these equations.

The integral equation is discretized using the method of moments technique with m basis functions. Testing with delta functions and applying due care to the treatment of the singularity associated with the Hankel function [1], leads to the following matrix equation

$$\mathbf{Z}(k_b)\mathbf{v}(k_b) = \mathbf{b}(k_b) \tag{6}$$

where $\mathbf{b}(k_b)$ is the incident field vector and $\mathbf{Z}(k_b)$ is a $m \times m$ matrix containing coupling information between the basis functions[1]. Using the circular-cell approximation [1], the element in the ith row and jth column of $\mathbf{Z}(k_b)$ is given by

$$Z_{ij} = \frac{\eta\pi a_i}{2}J_1(k_b a_i)H_0^{(2)}(k_b|\mathbf{r} - \mathbf{r}'|) \quad i \neq j \tag{7}$$

and

$$Z_{ij} = \frac{\eta\pi a_i}{2}H_1^{(2)}(k_b a_i) - \frac{\jmath\eta\epsilon_c}{k_b(\epsilon_c - \epsilon_0)} \quad i = j \tag{8}$$

where J_1 is the bessel function of order 1, η is the background impedance and a_i denotes the equivalent radius of cell i. Equation (6) may be solved for $\mathbf{v}(k_b)$ to determine the total unknown current $J_z(\mathbf{r})$ throughout the scatterer. Once $\mathbf{v}(k_b)$ is obtained, other quantities, such as the RCS or the fields at points exterior to the scatterer, can be computed [1].

III. Review of Asymptotic Waveform Evaluation via Padé Approximation With Adaptive Zeta

The principle goal in AWE is to extract information about the system behavior over a wide frequency range from the solution at one or several frequency points [2], [3], [18]. This is possible because coefficients of the matrix equation, describing the system behavior, are known functions of frequencies.

The AWE method approximates the frequency response by expanding $\mathbf{v}(k_b)$ into a Taylor series around k_{b0}

$$\mathbf{v}(k_b) = \sum_{n=0}^{N}\mathbf{m}_n\beta^n \tag{9}$$

where $\mathbf{m}_n$ are the moments of $\mathbf{v}(k_b)$, N is the order of the Taylor series expansion, $\beta = (k_b - k_{b0})$ and k_{b0} is the wave

[1]We have made explicit the dependence on frequency through the wave number k_b.

number at the expansion frequency. By substituting (9) into (6), expanding the impedance matrix $\mathbf{Z}(k_b)$ and the excitation vector $\mathbf{b}(k_b)$ into a Taylor series, we can rewrite (6) as

$$\sum_{n=0}^{N} \mathbf{Z}^{[n]}\beta^n \sum_{n=0}^{N} \mathbf{m}_n\beta^n = \sum_{n=0}^{N} \mathbf{b}^{[n]}\beta^n. \tag{10}$$

Finally, equating the coefficients of equal powers of β on both sides of (10) yields the recursive relation for the moment vectors

$$\mathbf{m}_n = \mathbf{Z}^{-1}(k_{b0}) \left[\frac{\mathbf{b}^{[n]}(k_{b0})}{n!\xi^n} - \sum_{q=0}^{n} \frac{(1-\delta_q)\mathbf{Z}^{[q]}(k_{b0})\mathbf{m}_{n-q}}{q!\xi^q} \right] \tag{11}$$

where δ_q is the Kronecker delta and ξ is a scaling factor used to improve the conditioning of the Padé coefficient matrix [19][2]. Vector $\mathbf{b}^{[n]}(k_{b0})$ denotes the nth derivative with respect to k_b of $\mathbf{b}(k_b)$ evaluated at k_{b0}. Similarly $\mathbf{Z}^{[q]}(k_{b0})$ denotes the qth derivative of $\mathbf{Z}(k_b)$ computed at k_{b0}.

Once the moment vectors are obtained, the value of $\mathbf{v}(k_b)$ at other frequencies can be calculated using (9). However, the use of this expansion is limited to the radius of convergence of the Taylor series. In such cases, the rational function approach is used to improve the accuracy of the numerical solution. The Padé representations have a larger radius of convergence and therefore can provide broader extrapolation as they include poles as well as zeros in the response [2].

The AWE moment-matching subspace, $\mathbf{M}_n$, generated from the recursive (11), is given by the span of the columns of the matrix

$$\mathbf{M}_n = [\mathbf{m}_1, \mathbf{m}_2, \ldots, \mathbf{m}_n] \tag{12}$$

where $\mathbf{m}_n$ are the moment vectors. It has been well documented [2], [6], [3], [18], [20] that the process of sequentially evaluating $\mathbf{m}_n$ via (11) is inherently ill-conditioned leading to instability in the computation of the Padé approximation. In a direct implementation, finite precision arithmetic causes each newly created moment vector $\mathbf{m}_n$ to converge towards the eigenvector that is associated with the dominant eigenvalue of $\mathbf{Z}(k_{b0})$. As a result, the moments $\mathbf{m}_n$ contain only information corresponding to one eigenvalue of $\mathbf{Z}(k_{b0})$, even for small values of n. Consequently, the solution of the Padé approximation becomes unattainable, thus restricting its use to approximations of relatively low order, typically for values of $n < 15$. Hence, it is necessary to implement the construction of the moment vectors in a numerically stable way. This is generally done with the help of an orthogonalization process, whereby imposing an orthogonality relation upon the vectors maintains linear independence. Consequently, high order approximations can be constructed. This is described in Section V where the WCAWE is reviewed. The next section introduces how the frequency dependent variations in the dielectric properties can be accounted for in a frequency sweep analysis using MOR.

[2]It should also be noted that the Taylor series expands in term of the wave number instead of frequency to reduce the effect of scaling in the derivation of the moments [19].

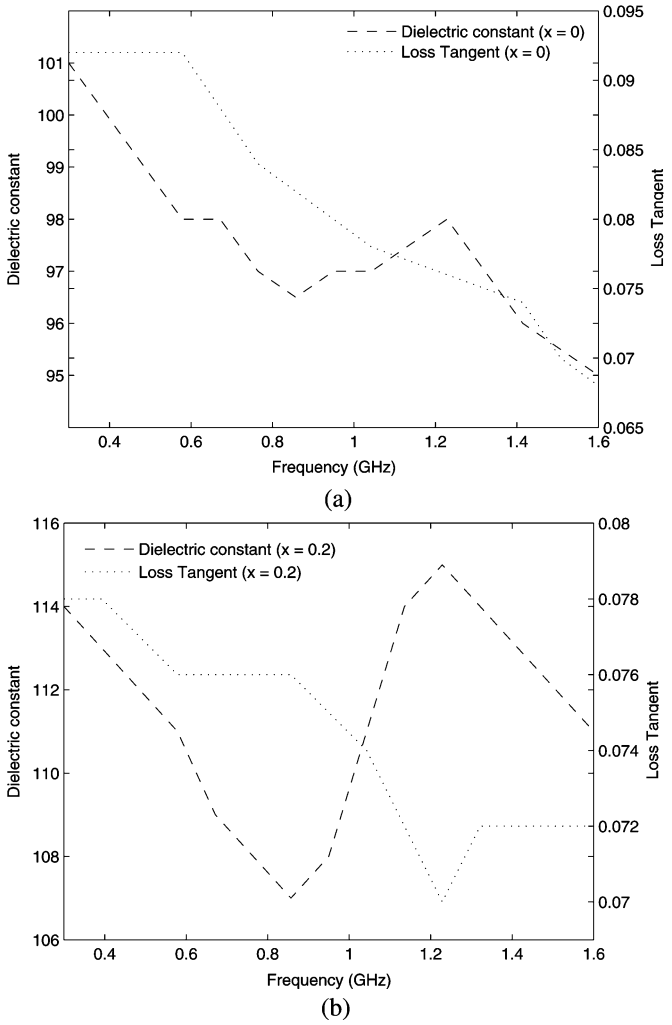

Fig. 1. Microwave dielectric properties of $Ba_xLa_4Ti_{2+x}O_{12+3x}$ as a function of frequency for two specific values of x. (a) Dielectric constant and loss tangent of $Ba_xLa_4Ti_{2+x}O_{12+3x}$ for $x = 0.0$, (b) dielectric constant and loss tangent of $Ba_xLa_4Ti_{2+x}O_{12+3x}$ for $x = 0.2$.

IV. Recursive Formulation of the Matrix Derivatives

In order to model the frequency dependant variations in ϵ evident in (1), (4), and (5), careful consideration needs to taken when differentiating (7) and (8). To model this dependence, initially a third-order polynomial is fitted to the tabulated dielectric properties of the ceramic $Ba_xLa_4Ti_{2+x}O_{12+3x}$ listed in [9] and illustrated in Fig. 1(a) and (b) for 2 distinct values of x. An analytical expression is independently fitted for both the real and imaginary permittivity of the form

$$\begin{aligned} \epsilon'(k_b) &= a'k_b^3 + b'k_b^2 + c'k_b + d' \\ \epsilon''(k_b) &= a''k_b^3 + b''k_b^2 + c''k_b + d'' \end{aligned} \tag{13}$$

where (a', b', c', d') and (a'', b'', c'', d'') are the polynomial constants for real and imaginary permittivity in each basis cell respectively. The following identities, gives the qth order recursive form of the derivatives of $a(k_b)$ expanded as a product [21]

$$\text{if } a(k_b) = b(k_b)c(k_b)$$

TABLE I
WELL-CONDITIONED ASYMPTOTIC WAVEFORM EVALUATION ALGORITHM (WCAWE)

$\tilde{\mathbf{m}}_1 = \mathbf{Z}_0^{-1}\mathbf{b}_0$
$\mathbf{U}_{[1,1]} = \|\tilde{\mathbf{m}}_1\|_2$
$\mathbf{m}_1 = \tilde{\mathbf{m}}_1\mathbf{U}_{[1,1]}^{-1}$
for $n = 2, \ldots, q$
  $\tilde{\mathbf{m}}_n = \mathbf{Z}_0^{-1}\left[\sum_{m=1}^{n-1} \mathbf{b}_m\mathbf{e}_1^T\mathbf{P}_{\mathbf{U}1}(n,m)\,\mathbf{e}_{n-m} - \mathbf{Z}_1\mathbf{m}_{n-1} - \sum_{m=2}^{n-1}\mathbf{Z}_m\mathbf{M}_{n-m}\mathbf{P}_{\mathbf{U}2}(n,m)\,\mathbf{e}_{n-m}\right]$
  for $\alpha = 1, \ldots, n-1$
    $\mathbf{U}_{[\alpha,n]} = \mathbf{m}_\alpha^H\tilde{\mathbf{m}}_n$
    $\tilde{\mathbf{m}}_n = \tilde{\mathbf{m}}_n - \mathbf{U}_{[\alpha,n]}\mathbf{m}_\alpha$
  end α
  $\mathbf{U}_{[n,n]} = \|\tilde{\mathbf{m}}_n\|_2$
  $\mathbf{m}_n = \tilde{\mathbf{m}}_n\mathbf{U}_{[n,n]}^{-1}$
end n.

then

$$a^{[q]}(k_b) = \sum_{p=0}^{q}\binom{q}{p} b^{[q-p]}(k_b)c^{[p]}(k_b) \tag{14}$$

or a quotient [21]

$$\text{if } a(k_b) = \frac{b(k_b)}{c(k_b)}$$

then

$$a^{[q]}(k_b) = \frac{1}{c(k_b)}\left[b^{[q]}(k_b) - \sum_{p=1}^{q} c^{[p]}(k_b)a^{[q-p]}(k_b)\right]. \tag{15}$$

Using (13) and the above identities the qth derivative with respect to k_b of the matrix entry $\mathbf{Z}_{i,j}(k_b)$, evaluated at k_{b0}, is given by

$$Z_{i,j}^{[q]} = \frac{\eta\pi a_i}{2}\sum_{p=0}^{q}\binom{q}{p} J_1(k_{b0}a_i)^{[p]}H_0^{(2)}(k_{b0}|\mathbf{r}_i - \mathbf{r}_j|)^{[q-p]} \quad i \neq j \tag{16}$$

and

$$Z_{i,j}^{[q]} = \frac{\eta\pi a_i}{2}H_1^{(2)}(k_{b0}a_i)^{[q]} - C_q \quad i = j \tag{17}$$

where

$$C_q = \frac{1}{k_{b0}(\epsilon_{ci}(k_{b0}) - \epsilon_0)}\left[(\jmath\eta\epsilon_{ci}(k_{b0}))^{[q]} - \left[\sum_{j=1}^{q}\left[\sum_{p=0}^{j}\binom{j}{p}(k_b)^{[p]}(\epsilon_{ci}(k_{b0}) - \epsilon_0)^{[j-p]}\right]C^{[q-j]}\right]\right]. \tag{18}$$

In particular

$$(\jmath\eta\epsilon_{ci}(k_{b0}))^{[q]} = (\jmath)^{[q]}\left(\left(a_i'k_b^2 + b_i'k_b + c_i'\right)^{[q]} - \jmath\left(a_i''k_b^2 + b_i''k_b + c_i''\right)^{[q]}\right). \tag{19}$$

For the sake of clarity, $\mathbf{Z}^{(q)}(k_{b0}), \mathbf{b}^{(q)}(k_{b0})$ and $\mathbf{v}(k_b)$ will be denoted by $\mathbf{Z}_q$,$\mathbf{b}_q$ and $\mathbf{v}$, respectively. The following recursive relation is used [22]

$$\Psi_v^{(q)} = \frac{1}{2^q}\sum_{p=0}^{q}(-1)^{(p+2)}\binom{q}{p}\Psi_{v-q+2p} \tag{20}$$

when differentiating the Bessel and Hankel functions, where $\Psi_v^{(q)}$ denotes the qth derivative of $J, Y, H^{(1)}, H^{(2)}$ of order v.

V. WELL-CONDITIONED ASYMPTOTIC WAVEFORM EVALUATION

A proposed approach that avoids the numerical ill-conditioning of the AWE is the WCAWE [5], [18], [20], which introduces correction factors that eliminate ill-conditioning in order to obtain high-order approximations in a numerically stable manner. Orthogonalized Krylov subspace methods such as the Galerkin asymptotic waveform evaluation (GAWE) [23], [24], can also construct an arbitrarily high-order stable approximation but in some cases may not match moments. The WCAWE process, outlined in Table I, rectifies this issue by the introduction of correction terms in the orthogonalization process. The columns of $\mathbf{M}_n$ from (12) are constructed iteratively by utilizing a modified Gram-Schmidt process. This procedure is used to orthogonalize $\mathbf{m}_n$ into the basis

$$\tilde{\mathbf{M}}_{n-1} = [\tilde{\mathbf{m}}_1, \tilde{\mathbf{m}}_2, \ldots, \tilde{\mathbf{m}}_{n-1}]. \tag{21}$$

This is achieved by computing the orthogonal projection of $\tilde{\mathbf{m}}_n$ onto $\text{span}\{\mathbf{m}_1\ \mathbf{m}_2\ \cdots\ \mathbf{m}_{n-1}\}$. This projection is subtracted from the original vector and the result is normalized to obtain $\mathbf{m}_n$. This is, by construction, orthogonal to all previously computed vectors $\tilde{\mathbf{m}}_1, \tilde{\mathbf{m}}_2, \ldots, \tilde{\mathbf{m}}_{n-1}$ and has unit norm. In this way, the orthogonality of the basis vectors is guaranteed and the moment-matching process can be maintained. The resultant vector generated in Table I is given by [5], [18], [20]

$$\tilde{\mathbf{m}}_n = \mathbf{Z}_0^{-1}\left(\sum_{m=1}^{n-1}\left(\mathbf{b}_m\mathbf{e}_1^T\mathbf{P}_{\mathbf{U}1}(n,m)\mathbf{e}_{n-m}\right) - \mathbf{Z}_1\mathbf{m}_{n-1} - \sum_{m=2}^{n-1}\mathbf{Z}_m\mathbf{M}_{n-m}\mathbf{P}_{\mathbf{U}2}(n,m)\,\mathbf{e}_{n-m}\right) \tag{22}$$

TABLE II
CPU TIME ANALYSIS—m = SIZE OF MOM MATRIX, n_0 = NUMBER OF MOMENTS, t_m = CPU TIME IN SECONDS TO GENERATE MOM MATRICES FOR ALL SAMPLES, n_s—NUMBER OF FREQUENCY SAMPLES, t_g = CPU TIME IN SECONDS TO GENERATE MOMENTS, n_m = NUMBER OF FREQUENCY SAMPLES CONVERGED TO PREDEFINED TOLERANCE $\mathrm{tol}_{rn} = 10^{-2}$, t_s = AVERAGE CPU TIME IN SECONDS TO SOLVE FOR RCS AT EACH FREQUENCY, t_t = TOTAL CPU TIME IN SECONDS TO GENERATE AND SOLVE CASE STUDY PROBLEM

Legend	Technique (Case study 1 - $f = 0.4 : 0.5$ GHz, $\lambda_0 = 0.6m$, $r = 0.2m$)						
	MoM	Padé via AWE with adaptive ζ			WCAWE		
Order	m = 1020	n_o = 15	n_o = 10	n_o = 5	n_o = 15	n_o = 10	n_o = 5
$t_m(s)$	5829	-	-	-	-	-	-
n_s	145	145	145	145	145	145	145
$t_g(s)$	-	4385	1333.2	213.2	4390	1334.9	213.23
n_m	-	113	81	33	145	113	60
$t_s(s)$	2.54	0.05	0.05	0.05	0.08	0.08	0.08
$t_t(s)$	6197.3	4392.25	1340.45	220.45	4402	1346.5	224.83
Speed-up	-	1.41	4.62	28.11	1.41	4.6	27.56

where $\mathbf{e}_r$ is the $m \times 1$ vector with the rth component equal to unity and all others equal to zero. $\tilde{\mathbf{M}}_n$ and $\mathbf{M}_n$ are related by an $n \times n$ upper triangular, nonsingular matrix $\mathbf{U}$ (Table I) created by the coefficients of the Gram-Schmidt process

$$\mathbf{M}_n = \tilde{\mathbf{M}}_n \mathbf{U}^{-1}. \tag{23}$$

The correction term in (22) is given by [5], [18], [20]

$$\mathbf{P}_{\mathbf{U}w}(n,m) = \prod_{t=w}^{m} \mathbf{U}^{-1}_{[t:n-m+t-1,t:n-m+t-1]} \tag{24}$$

where $w = 1$ or 2. $\mathbf{P}_{\mathbf{U}w}(n,m)$ is constructed from blocks extracted from the mapping matrix $\mathbf{U}$ created by the coefficients of the Gram-Schmidt process. The $\mathbf{P}_{\mathbf{U}w}(n,m)$ matrix tracks the mapping from one vector space to another for the higher-order terms in the WCAWE process.

Ultimately, this process results in the approximation to the solution vector $\mathbf{v}_n$ for any frequency f in the range $f_{\min} \leqslant f \leqslant f_{\max}$ given by [5], [18], [20]

$$\mathbf{v}_n = \mathbf{M}_n \left(\sum_{m=0}^{N} \beta^m \mathbf{M}_n^T \mathbf{Z}_m \mathbf{M}_n \right)^{-1} \left(\sum_{m=0}^{N} \beta^m \mathbf{M}_n^T \mathbf{b}_m \right). \tag{25}$$

Clearly, (25) can be used to efficiently solve over a wide range of frequencies as it requires the inversion of a matrix of order $n \ll m$ for each frequency value.

A. Multipoint Extension

In order to extend the bandwidth in a frequency sweep, a multipoint approach should be implemented. Determining the optimum size of the approximation order n at each expansion point will result in a more efficient approximation. As evident in Table II (line $t_g(s)$), the majority of the computational cost of generating the approximation is due to the calculation of the derivatives. Fig. 2(f) illustrates the CPU break-even analysis comparing the cost of generating the derivatives to the number of frequency samples required. As the number of moments increase there is a rapid increase in the number of samples required to achieve a CPU saving using the WCAWE over the MoM. This data can be used as a guide to determine the maximum number of moments that should be matched at each expansion point.

After determining the maximum value for n at the central expansion point β_0, one must consider if further expansion points are required and where they must be located, such that the approximate solution can converge to a pre-specified tolerance. After β_0 has been chosen, the approximate solution $\mathbf{v}$ and the relative residual [5], [25], [24]

$$R_n = \frac{\|\mathbf{r}_n\|_2}{\left\| \sum_{j=0}^{N} \beta^j \mathbf{b}_j \right\|_2} \tag{26}$$

should be generated for all frequencies f in the range $f_{\min} \leqslant f \leqslant f_{\max}$ where

$$\mathbf{r}_n = \sum_{m=0}^{N} (\beta^m \mathbf{Z}_m)\mathbf{v}_n - \sum_{m=0}^{N} \beta^m \mathbf{b}_m. \tag{27}$$

If $R_n < \mathrm{tol}_{rn}$ for some tolerance value tol_{rn}, the corresponding frequency f is marked as converged for $\mathbf{v}_n$. If either $f_{\min}$ or $f_{\max}$ are not converged another expansion point is selected at the centre of region in which convergence did not take place and R_n generated. The unconverged region is continually divided and tested until all values of f are marked as converged.

VI. NUMERICAL RESULTS AND VALIDATIONS

In this section, the RCS is calculated for profiles of varying contrast with the objective of validating the WCAWE by comparison with the method of moments. The effect of the frequency dependent variation in the dielectric properties of the ceramic $\mathrm{Ba_xLa_4Ti_{2+x}O_{12+3x}}$ for various values of x is examined in a frequency sweep analysis.

A. Case Study 1: Homogeneous Cylinder—Medium 1

We initially consider a homogeneous cylinder of radius $r = \lambda_0/3 = 0.2m$, centred at the origin and assumed to be embedded in free space. The frequency dependent dielectric prop-

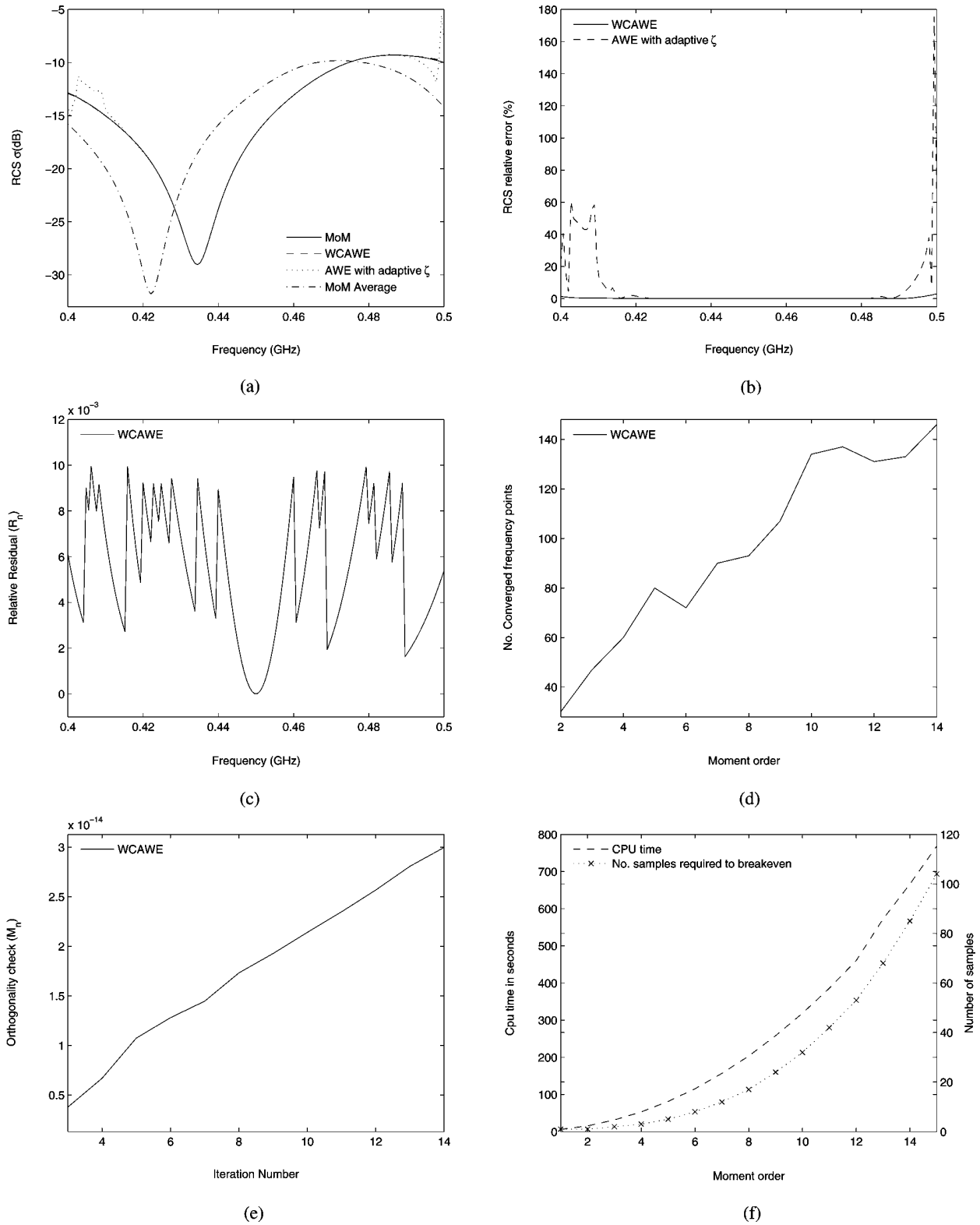

Fig. 2. Case study 1: Single Point Expansion.—Homogeneous cylinder. (a) $\sigma_{\mathrm{TM}}(\Phi)$ RCS frequency sweep comparing MoM, Padé via AWE with adaptive zeta, WCAWE, and MoM using average valve for dielectric constant $\epsilon' = 104.46$ and $\tan\delta = 0.087$ (Fig. 1(a) $x = 0.0$), (b) Percentage relative error for Fig. 2(a), (c) Relative residual R_n for WCAWE. (d) Number of converged frequency points at each moment for WCAWE. (e) loss of orthogonality over iteration process. (f) CPU break-even analysis.

erties for this object is illustrated in Fig. 1(a) for $x = 0$. The structure is illuminated by a transverse magnetic (TM^z) wave emanating from a line source located at $(-10, 0)$. The cylinder is discretized using $m = 1020$ cells and the RCS was computed over a band of frequencies $f = 400 : 500$ MHz with 0.68 MHz increments for a monostatic setup $\phi = 0$.

Fig. 2(a) and (b) shows the RCS and associated percentage relative error obtained in comparing the MoM against the Padé

via AWE with adaptive Zeta and the WCAWE for $n = 15$. To demonstrate the significant effect of the frequency dependence of the permittivity ϵ, the RCS is calculated using the MoM with an average value for the dielectric properties for $x = 0$ Fig. 1(a) ($\epsilon' = 104.46, \tan\delta = 0.087$). This is evident in Fig. 2(a) where this approximation results in an significant error over the entire frequency range, thereby justifying the need to account for the frequency dependence of the dielectric properties.

Although scaling reduces the ill-conditioning of the Padé coefficient matrix as discussed in Section III, these strategies still result in significant round-off error for relatively small values of n. From Fig. 2(a) and (b), it is clear the WCAWE out-performs the Padé via AWE with adaptive Zeta, duplicating the reference solution over the entire band of frequencies to within a 1% relative error. This is confirmed in Fig. 2(c), where the relative residual R_n (26) demonstrates that each sample in the range $f = 400 : 500$ MHz has converged to a pre-specified $\mathrm{tol}_{rn} = 10^{-2}$.

As an indicator of the rate of convergence of the frequency points to the $\mathrm{tol}_{rn} = 10^{-2}$ over the iteration process, Fig. 2(d) depicts the number of converged frequency points that has been achieved in total at each iteration. From this figure, we note the WCAWE process results in a regular addition of converged frequency point at each iteration.

Fig. 2(e) illustrates the loss of orthogonality of a computed set of moments $\mathbf{m}_n$ at each iteration step $||\mathbf{I}_n - \mathbf{m}_n^H \mathbf{m}_n||_2$, where $\mathbf{I}_n$ is a $n \times n$ identity matrix. From this figure, it is clear that the computed moments remain close to machine precision ensuring that each new moments contain additional new useful information.

The CPU time associated with the solution of the RCS for the MoM, Padé via AWE with adaptive Zeta and WCAWE is given in Table II. It is evident from this table that the WCAWE significantly decreases the computational expense associated with the direct solution of each frequency sample in a sweep analysis. Additionally, it is clear from this table that as the number of moments increase the WCAWE technique significantly outperforms the AWE in the amount of frequency points which have converged to tol_{rn}. The Padé via AWE with adaptive Zeta and WCAWE CPU times are similar due to the additional times required to scale the Padé via AWE with adaptive Zeta moments. The main computational overhead is due to the generation of the derivatives and this is clearly illustrated in Fig. 2(f). However, as the derivatives need only be calculated once, there is minimal computational expense required for all subsequent solutions. Additionally, this figure indicates the number of frequency samples required to achieve a computational saving.

B. Case Study 2: Inhomogeneous Cylinder—Medium 1, 2

In the second example, a similar numerical experiment is conducted for an inhomogeneous circular cylinder composed of two concentric regions centred at the origin, with radius ($r_1 = \lambda_0/3 = 0.2m$, medium 1), ($r_2 = \lambda_0/6$, medium 2). The cylinder is discretized using $m = 1020$ cells and the RCS was computed over a band of frequencies $f = 400 : 600$ MHz with 0.68 MHz increments for a monostatic setup $\phi = 0$.

Fig. 3(a) show the RCS results obtained in comparing the MoM results against the WCAWE ($n = 12$) and using an average value for the dielectric properties in medium 1 and 2 with one expansion point at $\sigma_1 = 500$ MHz (medium $1 - \epsilon' = 104.46, \tan\delta = 0.087$, Fig. 1(b) $x = 0.0$ and medium $2 - \epsilon' = 119.43, \tan\delta = 0.079$, Fig. 1(a) $x = 0.2$). The WCAWE algorithm duplicates the reference solution over the band of frequencies $f = 450 : 540$ MHz to within an 1% relative error. Again, we note the need to include the frequency dependent variation of the dielectric properties in the WCAWE process. This is shown in Fig. 3(a) where there is a significant error over the entire frequency range for the MoM solution based on the average value for the complex permittivity.

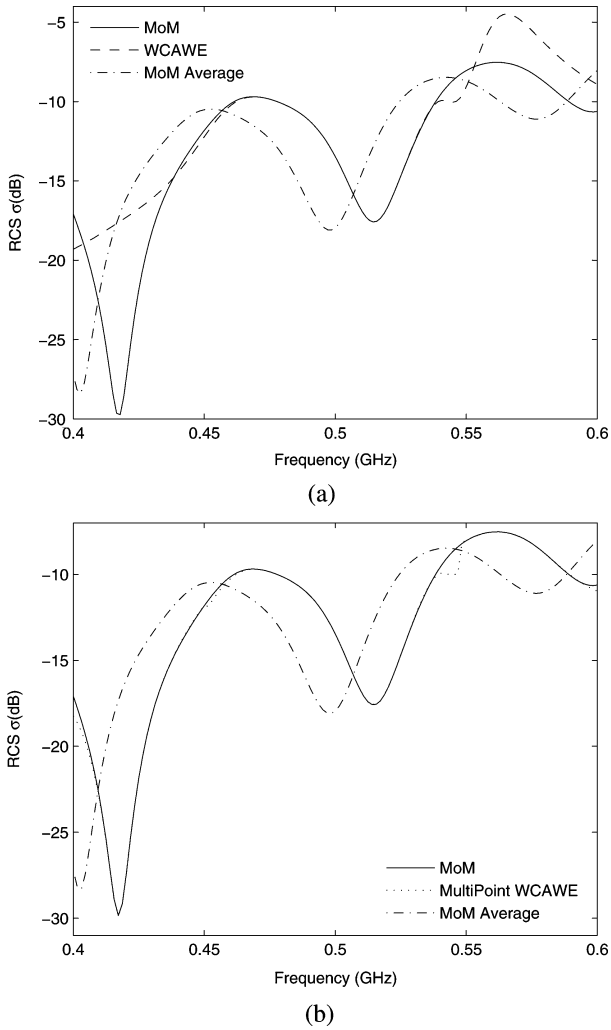

Fig. 3. Case study 2: Multi point expansion—Inhomogeneous cylinder. (a) $\sigma_{\mathrm{TM}}(\Phi)$ RCS frequency sweep comparing MoM, WCAWE, and MoM using average valve for dielectric constant—Medium 1, $\epsilon' = 104.46$ and $\tan\delta = 0.087$ (Fig. 1(a) $x = 0.0$) Medium 2, Medium 1, $\epsilon' = 119.43$ and $\tan\delta = 0.079$ (Fig. 1(a) $x = 0.2$), (b) Multipoint $\sigma_{\mathrm{TM}}(\Phi)$ RCS frequency sweep using MoM, WCAWE and MoM using average value for dielectric constant ($\sigma_1 = 500$ MHz $n_1 = 12, \sigma_2 = 425$ MHz $n_2 = 6, \sigma_3 = 574$ MHz $n_3 = 5$).

In order to achieve additional bandwidth, a multipoint WCAWE (MWCAWE) approach must be implemented. From Fig. 3(a), it is clear that for such an approach, we need to place two additional expansion points. These are automatically positioned at the centre of the two unconverged bands of frequency ($\sigma_2, \sigma_3 = 425\ 574$ MHz respectively) for ($n_2 = 6, n_3 = 5$). Fig. 3(b) indicate that the Multipoint WCAWE can provide

TABLE III
CASE STUDY 2 CPU TIME ANALYSIS

Legend	Technique (Case study 2 - $f = 0.4 : 0.6$ GHz)		
	MoM	WCAWE	MWCAWE
Order	m = 1020	n_0 = 12	n_o = 12 + 6 + 5 = 23
$t_m(s)$	5829	-	-
n_s	145	145	145
$t_g(s)$	-	2337	2768
n_m	-	66	145
$t_s(s)$	2.54	0.08	0.08
$t_t(s)$	6197.3	2348.6	2779.6
Speed-up	-	2.64	2.22

accurate and robust fast frequency sweeps in broadband applications.

The CPU results using the WCAWE and MWCAWE is compared with the MoM direct calculation to demonstrate the efficiencies of these approaches, as shown in Table III. It can be seen that using the MWCAWE is approximately 2.22 times faster while achieving within 1% relative error over the entire frequency range. Although multiple expansion points with low order moments can significantly reduce the CPU times, it should be noted that this approach can become computationally expensive for large scale simulations. This is due to the need to make and invert a $\mathbf{Z}$ matrix at the expansion frequency for each new expansion point.

VII. CONCLUSION

A fast frequency sweep method for a volume electric field integral equation formulation for inhomogeneous lossy dielectric objects has been demonstrated using the WCAWE approach. The WCAWE method provides the flexibility needed to efficiently handle the short comings of the AWE with Padé; specifically, the loss of accuracy as n increases due to the explicit moment-matching process and the ill-conditioned Padé coefficient matrix. We have demonstrated that a significant reduction in the system size can be achieved for varying contrast profiles, while still resulting in an accurate approximation over a wide frequency range. Notably, the need to account for the frequency dependence of the permittivity and conductivity parameters in frequency sweep analysis has been demonstrated. Examples are presented which demonstrate that the WCAWE can produce a numerically stable and robust high order approximation from a single expansion point as compared to the Padé via AWE with adaptive zeta. It has been shown that in order to achieve a much broader bandwidth, a multipoint approach is necessary to produce an efficient and accurate response throughout the entire bandwidth.

REFERENCES

[1] A. F. Peterson, S. L. Ray, and R. Mittra, "Computational methods for electromagnetics," in *IEEE Press Series on Electromagnetic Wave Theory*, 1st ed. Piscataway, NJ: Wiley-IEEE Press, 1997.

[2] B. Fasenfest, J. D. Rockway, N. J. Champagne, and R. M. Sharpe, "A generalized fast frequency sweep algorithm for coupled circuit-EM simulations," in *Proc. IEEE Antennas Propag. Soc. Int. Symp.*, Jun. 20–25, 2004, vol. 4, pp. 3944–3947.

[3] C. J. Reddy, M. D. Deshpande, C. R. Cockrell, and F. B. Beck, "Fast RCS computation over a frequency band using method of moments in conjunction with asymptotic waveform evaluation technique," *IEEE Trans. Antennas Propag.*, vol. 46, no. 8, pp. 1229–1233, 1998.

[4] K. Gallivan, E. Grimme, and P. Van Dooren, "Pade approximation of large-scale dynamic systems with Lanczos methods," in *Proc. 33rd IEEE Conf. Decision Contr.*, Dec. 14–16, 1994, vol. 1, pp. 443–448.

[5] R. D. Slone, "Fast frequency sweep model order reduction of polynomial matrix equations resulting from finite element discretizations," Ph.D. dissertation, Ohio State Univ., Columbus, 2002.

[6] R. Achar and M. S. Nakhla, "Simulation of high-speed interconnects," , vol. 89, no. 8, pp. 1230–1230, Aug. 2001.

[7] J. R. Phillips, E. Chiprout, and D. D. Ling, "Efficient full-wave electromagnetic analysis via model-order reduction of fast integral transforms," in *Proc. 3rd Design Automation Conf.*, Jun. 3–7, 1996, pp. 377–382.

[8] H. Yamadaa, T. Okawaa, T. Tohdob, and H. Ohsat, "Microwave dielectric properties of $Ba_xLa_4Ti_{3+x}O_{12+3x}(x = 0.0–1.0)$ ceramics," *J. Eur. Ceramics Soc.*, vol. 26, pp. 2059–2062, 2006.

[9] S. B. Narang, D. Kaura, and S. Bahela, "Dielectric properties of lanthanum substituted barium titanate microwave ceramics," *J. Eur. Ceramics Soc.*, vol. 60, no. (25–26), pp. 3179–3182, Nov. 2006.

[10] C. Kittel, *Introduction to Solid State Physics*, 8th ed. New York: Wiley, 2005.

[11] M. Golio, *The RF and Microwave Handbook*. Boca Raton, FL: CRC Press, 2001.

[12] G. I. Torgivnikov, *Dielectric Properties of Wood and Wood-Based Materials*. New York: Springer-Verlag, 1993.

[13] D. Pena, R. M. Feick, H. D. Hristov, and W. Grote, "Measurement and modeling of propagation losses in brick and concrete walls for the 900-MHz band," *IEEE Trans. Antennas Propag.*, vol. 51, no. 1, pp. 31–39, Jan. 2003.

[14] A. Muqaibel, A. Safaai-Jazi, A. Bayram, A. M. Attiya, and S. M. Riad, "Ultrawideband through-the-wall propagation," *Proc. IEE Microw., Antennas Propag.*, pp. 581–588, 2005.

[15] D. K. Cheng, *Field and Wave Electromagnetics*, ser. Series in Electrical Engineering, 2nd ed. Reading, MA: Addison-Wesley, 1992.

[16] C. A. Balanis, *Advanced Engineering Electromagnetic*. New York: Wiley, 1989.

[17] R. Lovell, "Application of Kramers–Kronig relations to the interpretation of dielectric data," *J. Phys. C: Solid State Phys.*, vol. 7, pp. 4378–4384, 1974.

[18] J. X. Wan and C.-H. Liang, "Rapid solutions of scattering from microstrip antennas using well-conditioned asymptotic waveform evaluation," in *Progr. Electromagn. Res.*, 2004, vol. PIER 49, pp. 39–52.

[19] P. Feldmann and R. W. Freund, "Efficient linear circuit analysis by Padé approximation via the Lanczos process," *IEEE Trans. Comput.-Aided Design*, vol. 14, pp. 137–158, 1993.

[20] R. D. Slone, R. Lee, and J.-F. Lee, "Well-conditioned asymptotic waveform evaluation for finite elements," *IEEE Trans. Antennas Propag.*, vol. 51, no. 9, pp. 2442–2447, Sep. 2003.

[21] A. Jorba and M. Zou, "A software package for the numerical integration of ODEs by means of high-order Taylor methods," *Experiment. Math.*, vol. 14, p. 99, 2000.

[22] M. Abramowitz and I. A. Stegun, *Handbook of Mathematical Functions with Formulas, Graphs, and Mathematical Tables*, 9th ed. New York: Dover, 1964.

[23] R. D. Slone, R. Lee, and J.-F. Lee, "Terminating the iterative process for the Galerkin asymptotic waveform evaluation model order reduction technique," in *Proc. IEEE Antennas Propag. Soc. Int. Symp.*, Jul. 8–13, 2001, vol. 3, pp. 200–203.

[24] R. D. Slone, R. D. Slone, R. Lee, and J.-F. Lee, "Multipoint Galerkin asymptotic waveform evaluation for model order reduction of frequency domain fem electromagnetic radiation problems," *IEEE Trans. Antennas Propag.*, vol. 49, no. 10, pp. 1504–1513, 2001.

[25] R. D. Slone, R. Lee, and J.-F. Lee, "Automating multipoint Galerkin awe for a FEM fast frequency sweep," *IEEE Trans. Antennas Propag.*, vol. 38, no. 2, pp. 637–640, Mar. 2002.

Patrick J. Bradley was born in 1981. He received the B.Eng. degree in mechatronic engineering from the Dublin City University, Ireland, in 2004 were he is currently working toward the Ph.D. degree.

Since 2005, he has been affiliated with the RF modeling and simulation group at Dublin City University. His field of interest include model order reduction techniques and electromagnetic wave propagation modeling using integral equations.

Conor Brennan was born in Dublin, Ireland, in 1972. He received the B.A.(Mod) degree in mathematics and the Ph.D. degree from Trinity College, Dublin University, in 1994 and 1998, respectively.

He has been a Lecturer in the School of Electronic Engineering, Dublin City University (DCU) since 2003, where he is a member of the Network Innovation Centre within DCU's Research Institute for Networks and Communications Engineering (RINCE). He is also a founding member of DCU's Centre for Scientific Computing and Complex Systems Modelling. His research interests are electromagnetic wave propagation modeling for wireless systems, numerical techniques for integral equation modeling of EM wave scattering and energy-efficient communication techniques for low power wireless systems.

Marissa Condon received the B.E. degree (hons) in 1995 from the National University of Ireland, Galway, and the Ph.D. degree in 1998 from the National University of Ireland.

After receiving the Ph.D., she worked in the National Grid of the Electricity Supply Board of Ireland for two years before joining the School of Electronic Engineering, Dublin City University. She is joint leader of the RF Modelling and Simulation Group at Dublin City University. Her research interests are in the analysis and simulation of high-frequency circuits, the development of algorithms for CAD packages, nonlinear model reduction and the development of suitable macromodels for large-scale circuits and systems operating at high frequencies.

Dr. Condon is a Reviewer for IEEE-TCAS journals and ECCTD Conference.